RELIABILITY AND DURABILITY OF MATERIALS AND COMPONENTS FOR SOLID OXIDE FUEL CELLS

E. Lara-Curzio and M. Radovic
Beth Armstrong, Claudia Walls, Michael Lance, Peter Tortorelli, Shirley Waters, Larry Walker, and Amanda Murphy
Technical Contributors

1. INTRODUCTION

Fuel cells will play an important role in securing the energy future of the U.S. by providing efficient, environmentally friendly electrical energy. The Solid State Energy Conversion Alliance (SECA) is a unique alliance between government, industry, universities and National Laboratories to promote the development of solid oxide fuel cells (SOFC) as an affordable, clean and reliable source of electric power. The goal of SECA is to create solid oxide fuel cells (3–10 KW) that can be mass-produced in modular form at a target cost of $400/KW. As part of SECA's Core Technology Program, ORNL is supporting the industrial development teams to improve the durability and reliability of SOFC materials and components. In this report the results of activities related to evaluation of reliability and durability of materials and components for SOFC conducted at ORNL as part of the SECA Core Technology Program for the period of time of June 1, 2002–June 1, 2003 are presented.

2. CHANGES OF PHYSICAL AND MECHANICAL PROPERTIES DURING REDUCTION OF NIO/YSZ ANODE

One approach for the manufacture of SOFC stacks is based on the co-sintering of electrodes and electrolyte. Since these materials have different mechanical and physical properties, after sintering they will be subjected to residual stresses that could result in cracking and failure of the cell. Even if cells can be successfully co-sintered in air, subsequent processing steps (e.g., the reduction of NiO into Ni in the anode under constraints imposed by electrical interconnects and seals) may induce additional stresses that could compromise the structural and mechanical integrity of the stacks. During reduction, the physical and mechanical properties of the anode will change. Most significant is the shrinkage of the anode associated with the conversion of NiO into Ni. For the purpose of predicting the reliability and durability of SOFs, particularly during this step, it is necessary to quantify how the physical and mechanical properties of the anode change during reduction. During this reporting period a systematic study was initiated to determine and quantify how the physical and mechanical properties of anodes evolve during reduction.

2.1. KINETICS OF NiO/YSZ REDUCTION—THERMOGRAVIMETRIC ANALYSIS

A series of samples were prepared to study the evolution of the physical and mechanical properties of anodes after reduction. The samples consisted of a mixture of 75mol% NiO and the balance of 8mol%YSZ. In order to obtain a porous structure, 30vol% of organic pore former was added. Green samples were prepared by tape casting layers that were subsequently laminated into 1 mm thick specimens. Discs (nominal diameter 25.4 mm) were hot-knifed from the assembled green tapes prior to sintering at 1450°C in air. The porosity of the samples after sintering was determined to be 23.5±0.6 vol% by alcohol immersion according to ASTM standard C20-00.

The reduction of anode materials was studied using a termogravimetric unit with a detection limit of 0.1 mg at 600°C, 700°C, 750°C, and 800°C. Samples were placed on a quartz stand that was hung by a Pt suspension wire from the thermobalance. The stand with one sample was introduced in a reaction tube, which in turn was placed in a furnace. Before heating, the reaction tube was evacuated and then backfilled with argon. The sample was then heated up under a constant flow of argon up to the test temperature. After reaching thermal equilibrium, the gas was changed to a mixture of 4%H_2 and 96%Ar. A constant gas flow rate of 100 cc/min was maintained for the duration of the reduction process and the sample's weight change was recorded using an automatic data acquisition system. In addition to quantify the changes of the structural and mechanical properties as a function of the fraction of reduced NiO, a set of samples was reduced at 800°C for different periods of times.

The fraction of reduced NiO is plotted as a function of time for different reduction temperatures in Fig. 2.1. These curves exhibit two stages: in the first stage the rate of NiO reduction is liner at all

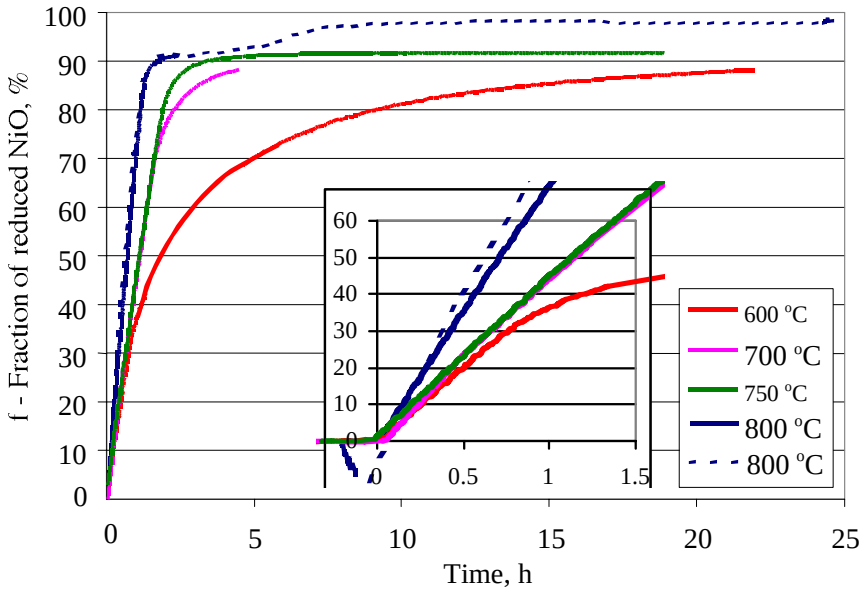

Fig. 2.1. Fraction of reduced NiO vs. time at different temperature. Insert shows magnified initial part of reduction curves.

temperatures above 600°C; in the second stage, the rate of reaction decreases continuously until the fraction of reduced NiO approaches 100%. At 600°C the rate of NiO reduction was found to decrease continuously from the start of the process. The transition from linear kinetics to semi-parabolic kinetics occurs at values of the fraction of reduced NiO that increase with temperature.

Figure 2.2 illustrates the development of the reduced layer on the surface of the anode samples during reduction in a mixture of 4%H_2-96%Ar at 800°C. The gray layers on both sides of the sample correspond to the reduced parts of the anode, while the green region in the center represents the unreduced parts of the anode. Figure 2.3. shows an SEM image, along with the WDS surface analysis of the same area, of a partially reduced NiO/YSZ anode. In this region three phases can be identified in the WDS image, namely NiO, Ni and YSZ, and thus it can be concluded that not all of NiO was reduced in the gray area. These

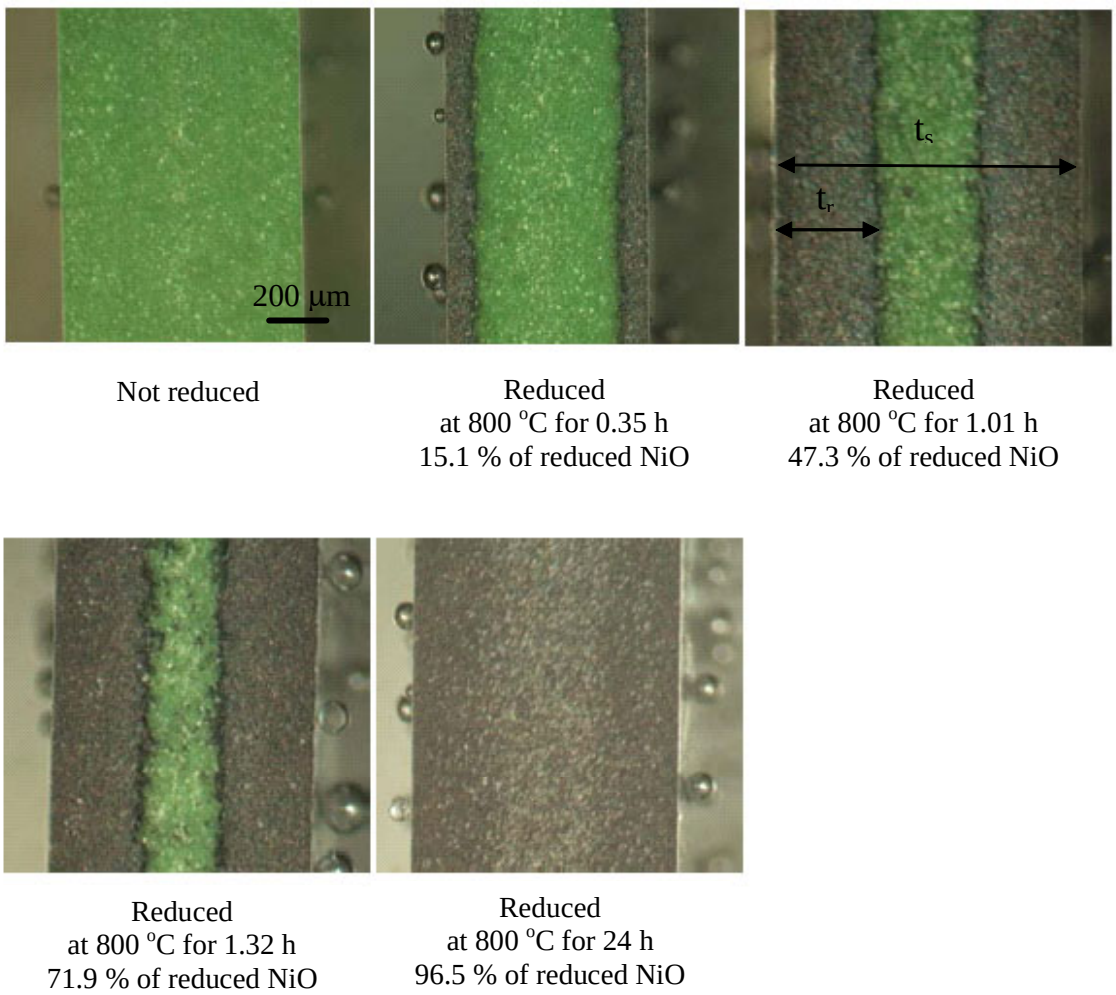

Fig. 2.2. Optical micrographs of polished cross-section of samples reduced in gas mixture of 4%H_2-96%Ar at 800°C for different periods of time.

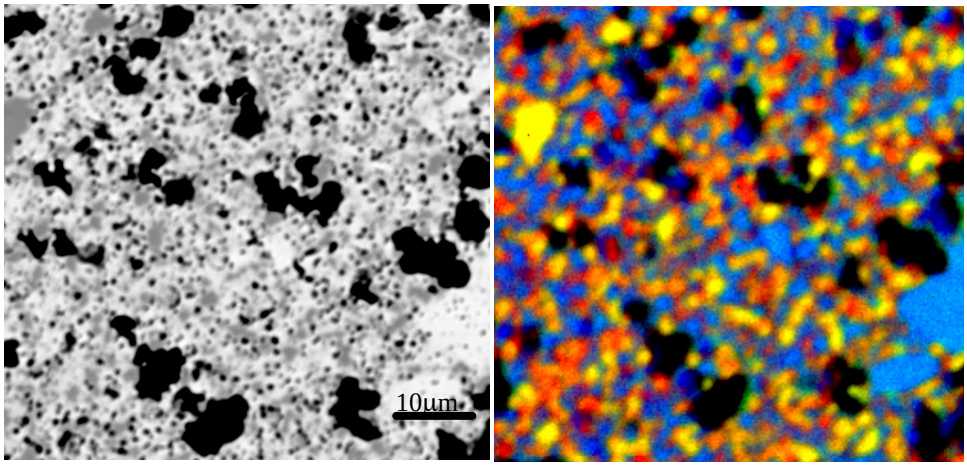

Fig. 2.3. Left: SEM secondary electron image of partially reduced NiO/YSZ anode. Right: WDS surface analysis of the same area. Blue—YSZ, red—pure Ni, yellow—NiO, black—pores. Fraction of reduced NiO in sample is 55 wt%.

results suggest that the partially reduced area grows rapidly at first (according to linear kinetics) and that further reduction of NiO grains, within the partially reduced (gray) area occurs as hydrogen reaches the interior of the sample during the second stage of the curves in Fig. 2.1. Thus, the transition point in the reduction kinetics appears to occur when the reduction fronts meet each other in the middle of the sample. Once this happens, only further reduction of the partially reduced NiO grains takes place at a much slower reduction rate.

The fraction of reduced NiO calculated after reduction for different times at 800°C is plotted in Fig. 2.4. Those data points (represented as blue diamonds) match well the continuous reduction curve obtained at 800°C for 24 hours. An Arrhenius analysis of the reduction rate, which was determined from the slop of the initial part of the ΔW_t vs. time curves showed that the activation energy associated with this process is 25.2 kJ/mol, which is comparable to published data for the reduction of pure NiO [1].

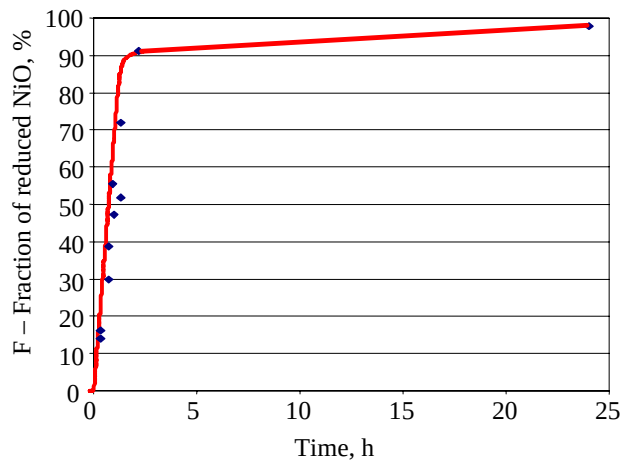

Fig. 2.4. Fraction of reduced NiO vs time at 800°C. Data points correspond to results obtained from interrupted reduction tests.

2.2. CHANGES OF POROSITY DURING THE REDUCTION OF NiO/YSZ ANODE

The porosity of samples after reduction in a gas mixture of 4%H_2-96%Ar was determined by alcohol immersion according to ASTM standard C20-00. Results are plotted in Fig. 2.5 as a function of the fraction of reduced NiO. These results demonstrate that there is a significant increase in the overall porosity of NiO/YSZ anodes as a result of reduction.

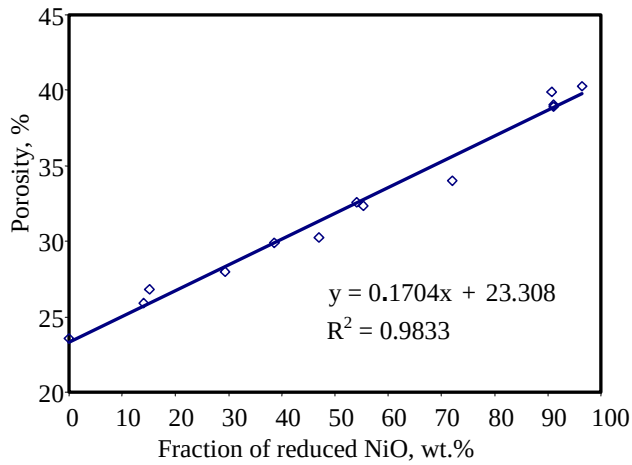

Fig 2.5. Overall porosity of the reduced NiO/YSZ samples as a function of the fraction of reduced NiO

2.3. CHANGES OF ELASTIC PROPERTIES DUE THE REDUCTION OF NiO/YSZ ANODE

The elastic properties of NiO/YSZ samples reduced for different periods of time in a gas mixture of 4%H_2-96%Ar were determined at room temperature by Impulse Excitation (IE) [2]. Young's and shear moduli values for reduced NiO/YSZ anode samples are plotted in Fig. 2.6 as a function of fraction of reduced NiO. These results show that the magnitude of Young's and Shear moduli decreases as the fraction of reduced NiO increases. After complete reduction, the magnitude of the elastic moduli are almost 50% of the values of the unreduced samples NiO/YSZ sample. Such a significant decrease of elastic moduli is a consequence of the increase in porosity and to a lesser degree to the difference in elastic modulus between NiO and Ni.

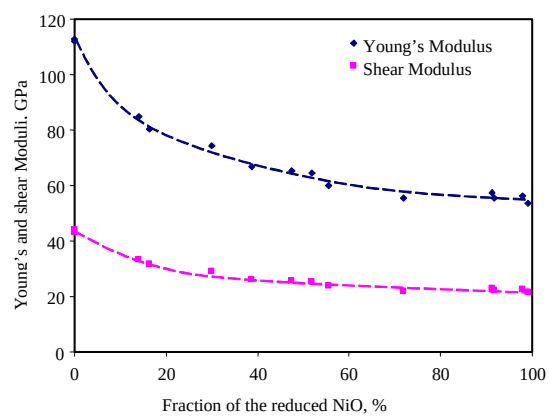

Fig. 2.6. Young's and shear moduli of reduced NiO/YSZ anode samples as a function of fraction of reduced NiO.

2.4. COEFFICIENTS OF THERMAL EXPANSION OF NiO/YSZ, Ni/YSZ, AND YSZ

The coefficients of thermal expansion (CTE) of 8mol% YSZ, 75mol%NiO/YSZ and fully reduced 75mol%NiO/YSZ (further denoted as Ni/YSZ) were determined by dilatometry. The 8mol%YSZ samples were tested in air up to 900°C at a heating rate of 2°C/min. The 75mol%NiO/YSZ sample was first heated in argon up to 800°C. Then, the gas flow was changed from pure argon to a gas mixture of 4%H_2-96%Ar. The length of the specimen was monitored for 24 hrs at 800°C and at the end of the time period the sample was cooled down at a rate of 2°C/min. Measurements of weight changes of the NiO/YSZ sample after reduction confirmed that sample was fully reduced. The coefficient of thermal expansion of 8mol%YSZ was 1.04×10^{-5} K^{-1}. The results for 75mol%NiO/YSZ before and after total reduction were found to be $1.18 \times 10^{-5}K^{-1}$ and $1.27–1.37 \times 10^{-5}K^{-1}$, respectively. These results are comparable to previously reported CTE's of 1.27 10^{-5} K^{-1} for 75mol%NiO/YSZ and 1.17 10^{-5} K^{-1} for NiO/YSZ cermets [3].

2.5. THERMAL DIFFUSIVITY OF NIO/YSZ, NI/YSZ AND YSZ

The thermal diffusivity of 8mol%YSZ and reduced and unreduced 75mol%NiO/YSZ was determined according to the laser flash method [4]. Results of thermal diffusivity measurements are presented in Fig. 2.7.

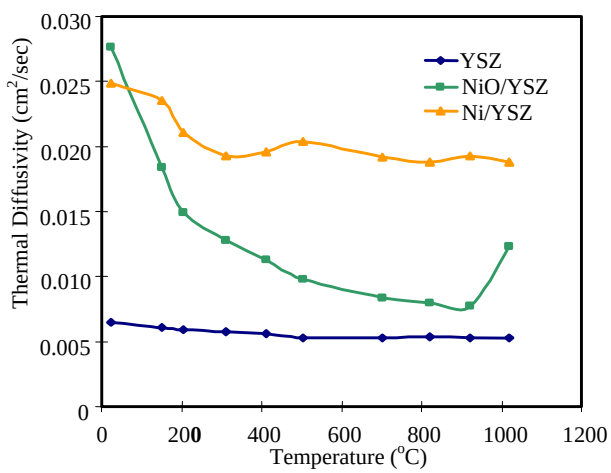

Fig. 2.7. Thermal diffusivity of YSZ, NiO/ YSZ and Ni/YSZ as a function of temperature.

2.6. MONITORING KINETICS DURING IN SITU REDUCTION OF NIO/YSZ USING RAMAN SPECTROSCOPY

Raman spectroscopy was used to monitor chemical changes in NiO/YSZ samples during *in situ* reduction. The experimental setup for in situ monitoring the reduction of NiO/YSZ anode material is schematically shown in Fig. 2.8. Raman spectra of two areas (labeled as 1 and 2 in Fig 2.9) were collected during the reduction process at 400°C. Fig. 2.9 shows optical micrographs and the corresponding Raman spectra as a function of reduction time. Raman spectra of areas 1 and 2 show characteristic peaks for NiO and cubic YSZ in both positions at room temperature and after reduction for 1 min at 400°C. After reduction at 400°C for 10 min the NiO peaks in spectra for area 1 have disappeared, while the peaks for NiO are barely detectable in position 2. After 22 min, only the characteristic peak for YSZ is present in the spectra obtained in position 1. This indicates

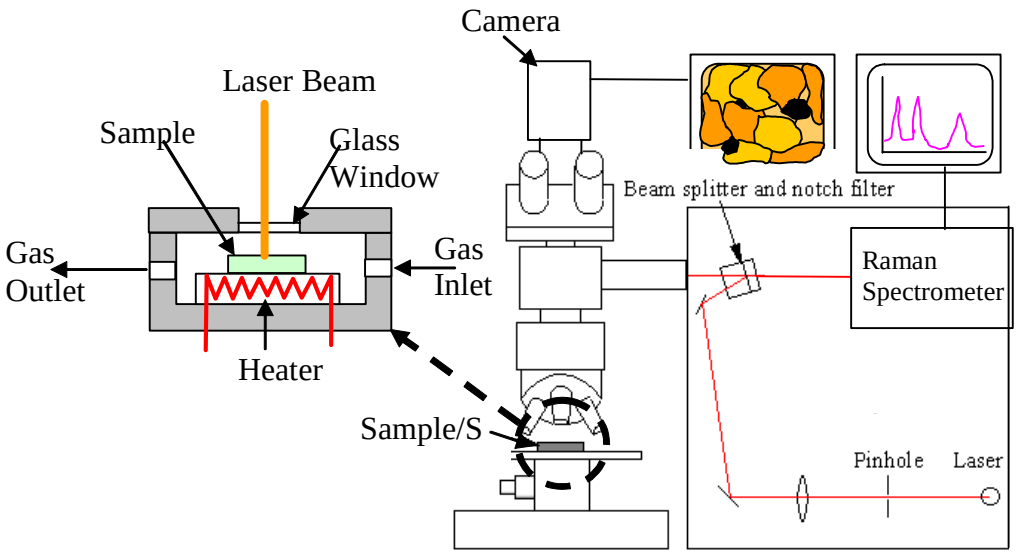

Fig. 2.8. Experimental setup for monitoring *in situ* reduction of NiO/YSZ using Raman Spectroscopy.

that position 2 was initially almost pure NiO, while position 1 was predominately YSZ. It has to be emphasized that these Raman spectra were obtained from the surface of the sample.

2.7. MONITORING STRESSES IN ELECTROLYTE DURING IN SITU REDUCTION OF NIO/YSZ USING RAMAN SPECTROSCOPY.

Attempts were made to monitor the evolution of stresses in 8%YSZ electrolytes bonded to NiO/YSZ anodes during reduction. However, the results from these experiments are still inconclusive since the position (wave number) of the cubic zirconia Raman peak as a function of temperature and stress has not been established yet. The results from these experiments will be valuable to validate predictions of internal stresses in SOFC during anode reduction

Fig. 2.9. Left: Optical micrographs of the NiO/YSZ sample after the different reduction times. Right: Corresponding Raman spectra of areas denoted as 1 (blue) and 2 (magenta) in the optical micrographs. Dashed lines in Raman spectra represent a standard position of Raman peaks for cubic YSZ. Solid vertical line in Raman spectra is a standard position of Raman peaks for NiO.

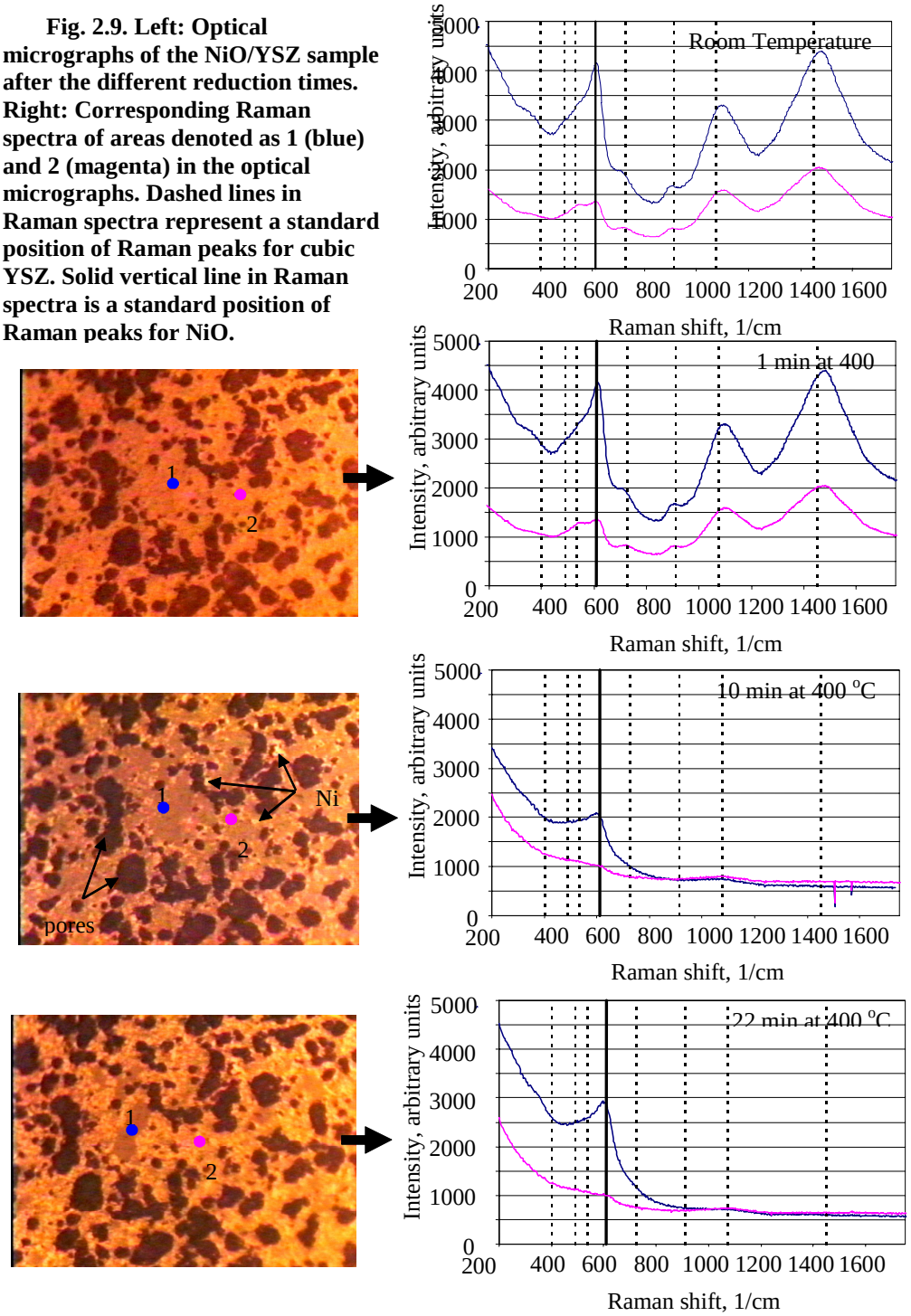

3. MECHANICAL CHARACTERIZATION OF ANODE AND ELECTROLYTE MATERIALS.

In this section the mechanical properties of electrolyte and anode materials, namely 8%YSZ, 75mol% NiO/YSZ and partially and fully reduced NiO/YSZ are presented. Young's and shear moduli, biaxial strength and fracture toughness were determined for all tested materials and the effect of testing temperature, porosity and sample's dimensions on mechanical properties were analyzed. The general characteristics of the samples evaluated in the present work are listed in Table 3.1.

Table 3.1. Characterized materials

	8YSZ			NiO/YSZ					
# of laminated layers	1	2	4	2	4	6	4	4	4
Nominal Thickness, mm	0.25	0.50	1.00	0.50	1.00	1.50	1.00	1.00	1.00
Pore former, vol%	0	0	0	30	30	30	25	20	0
Sintering conditions	1400°C for 2 h			1400°C for 2 h					
Measured porosity, %	7 ±1	7±1	6±1	–	23±1	–	20±1	17±1	7±1
Fraction of reduced NiO in fully reduced samples, %				–	98±2	–	99±1	–	–
Porosity of fully reduced NiO/YSZ samples					40±1.5	–	37±0.5	–	–
Fraction of reduced NiO in partially reduced samples, %				55±8			–	–	–

Green samples were prepared by tape casting layers that were subsequently laminated into specimens of the desired thickness. The porosity of the NiO/YSZ samples was tailored by varying the amount of organic pore former added to the tape cast formulation. Some of the NiO/YSZ samples were either partially or fully reduced in a gas mixture of 4%H_2-96%Ar.

The flexural strength of SOFC materials was determined under biaxial loading using the concentric ring-on-ring (ROR) flexural-loading configuration. Tests were carried out in air at room temperature, 600 and 800°C at a constant cross-head displacement rate of 1 mm/min. according to ASTM C1499-01.

The double torsion (DT) test was used to determine the fracture toughness, K_{IC}, of anode and electrolyte materials at ambient conditions.

3.1. ELASTIC PROPERTIES OF ANODE AND ELECTROLYTE MATERIALS FOR SOFC

The values of Young's and Shear Moduli obtained at room temperature are presented in Figs 3.1. and 3.2. as a function of porosity for 8YSZ and NiO/YSZ samples. The following two empirical relations expressing the effective modulus as a function of porosity were fitted to the experimental modulus vs. porosity data [5]:

linear $[\, M = M_0(1 - b_M\, p)\,]$ exponential $[\, M = M_0 \exp(-b_M\, p)\,]$

where M is modulus (G or E), at fractional porosity p ($0<p<1$), b_M is an empirical constant and M_0 is modulus of the sample with zero porosity. Fitting results are plotted in Figs. 3.1 and 3.2 as a solid black line for linear fitting and as a dashed black line for exponential fitting. Also, published results for similar materials [5] are plotted in Figs. 3.1 and 3.2 as a solid gray line for linear fitting and as a dashed gray line for exponential fitting. The fitting constants for the linear and exponential models are listed in Table 3.2. The estimated zero-porosity moduli values obtained in this work are different from previously published data [5] by less than 8%.

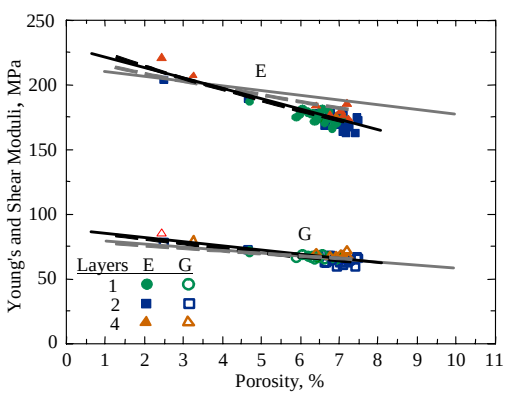

Fig. 3.1. Room temperature Young's and Shear Moduli of YSZ vs. porosity, for 1-layer, 2- and 4-layers samples.

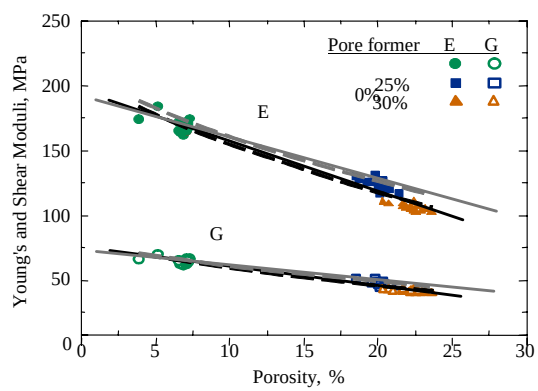

Fig. 3.2. Room temperature Young's and Shear Moduli of NiO/YSZ vs. porosity, for samples with 0, 25, and 30 % of pore former.

Table 3.2. Best fit values for zero-porosity moduli, E_0 , G_0 and porosity dependant constants (b_E and b_G) from this work and from Ref. [6]

			E_0, *MPa*	G_0, *MPa*	b_E	b_G
This work	YSZ	linear	229.8	88.2	3.8	3.7
		exponential	234.6	90.2	4.3	4.5
	NiO/YSZ	linear	195.4	75.1	2.0	1.9
		exponential	204.5	78.1	2.8	2.6
Ref. [5]	YSZ	linear	219.5	83.2	2.5	2.4
		exponential	220.3	83.5	2.7	2.6
	NiO/YSZ	linear	205.5	77.0	2.1	2.0
		exponential	207.1	78.0	2.5	2.4

3.2. WEIBULL ANALYSIS OF BIAXIAL STRENGTH OF YSZ ELECTROLYTE

The biaxial strength of YSZ samples with 1, 2 and 4 layers were determined at room temperature, 600 and 800°C. Altogether 161 samples were tested. The biaxial strengths were analyzed using Weibull statistics and values of the characteristic strength and Weibull modulus are listed in Table 3.3.

Table 3.3. Results of biaxial tests for YSZ

	T, °C	#	Characteristic Strength, MPa			Weibull modulus			Strength, MPa
			Avrg.	L.B.	U.B.	Avrg.	L.B.	U.B.	Avrg.± S.D.
4-layers	25	23	222.15	200.59	245.07	3.72	2.86	4.65	201.52±56.49
	600	21	132.81	123.69	142.12	5.65	4.24	7.26	123.14±23.50
	800	21	145.13	131.65	159.15	4.14	3.04	5.44	131.42±37.17
2-layers	25	15	176.23	159.51	193.50	4.89	3.38	6.74	161.15±39.15
	600	18	109.69	91.01	130.68	2.86	1.92	4.02	97.41±38.60
	800	12	146.15	132.39	160.25	6.86	4.15	10.39	136.40±23.78
1-layer	25	20	345.32	314.97	378.59	4.23	3.18	5.62	313.72±84.68
	600	15	140.83	133.55	148.50	8.46	6.08	11.78	133.02±18.61
	800	16	177.79	163.29	192.79	5.45	3.87	7.27	164.30±35.21

T—Temperature
Avrg.—Average value
L.B.—lower 95% Confidence bound
U.B.—Upper 95% Confidence bound
S.D.—Standard Deviation
#—number of tested samples

Weibull plots for biaxial strengths of characterized YSZ samples are shown in Figs. 3.3–3.5. These results suggest that the strength of YSZ decreases at 600°C, but increases at 800°C. However, the reasons for this dependence of the biaxial strength on temperature are not clear at this time. Also, these results indicate that the biaxial strength of multi-layered YSZ samples is lower than that of 1-layer samples, especially at room temperature. Extensive fractographic analysis of the fracture surfaces of these samples is underway with the objective of identifying the strength-limiting flaws. However, preliminary fractographic suggest that the occurrence of delaminations in multilayered samples might be associated with the observed reduction of strength.

3.3. WEIBULL ANALYSIS OF BIAXIAL STRENGTH OF NiO/YSZ PRECURSOR TO SOFC ANODE

The biaxial strength of NiO/YSZ samples was determined using samples of different porosity, namely 7, 17, 20 and 23 % at room temperature, 600 and 800°C. Also, the effect of sample thickness and number of layers were studied by evaluating samples with 2, 4 and 6 layers (Table 3.4.). Altogether 138 samples were evaluated. The biaxial strengths were analyzed using Weibull statistics and values of the

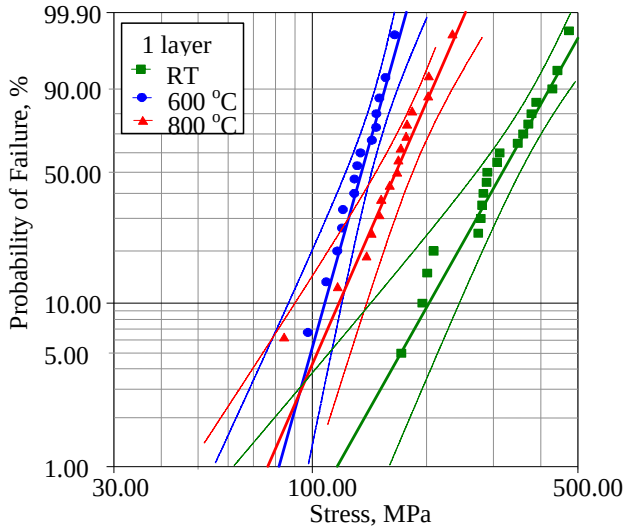

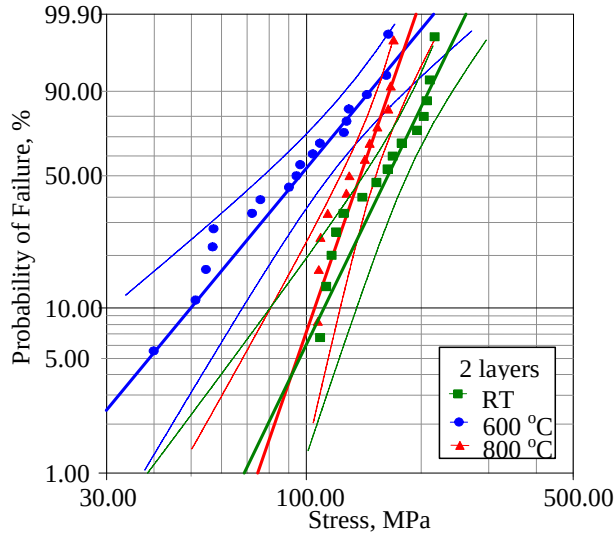

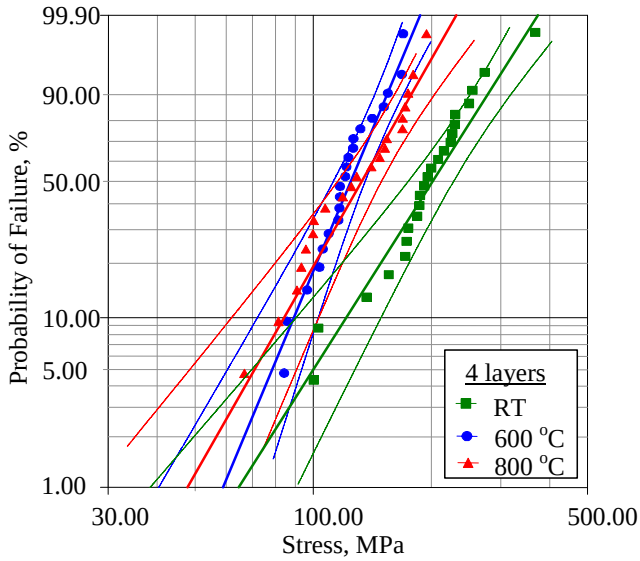

Figs. 3.3–3.5 Weibull plots for biaxial strength of YSZ samples with 1, 2 or 4 layers as a function of testing temperature. Dashed lines represent 95% confidence bounds/

characteristic strength and Weibull modulus are listed in Table 3.4. together with average strength values. Weibull plots for biaxial strengths of characterized NiO/YSZ samples are shown in Figs. 3.6–3.10.

These results suggest that the biaxial strength of NiO/YSZ has a weak temperature dependence. However, the decrease in biaxial strength with porosity is pronounced up to 17% of porosity, but the magnitude of the biaxial strength does not change considerably for higher levels of porosity. The only exception are 17% porous samples tested at 800°C. In that case, an exceptionally high characteristic strength was obtained. Also, it is worth noting that neither the number of layers nor the thickness of the samples have a significant influence on the magnitude of the biaxial strength of NiO/YSZ.

Table 3.4. Results of biaxial tests for NiO/YSZ

	T, °C	#	Characterist. Strength, MPa			Weibull modulus			Strength, MPa
			Avrg.	L.B.	U.B.	Avrg.	L.B.	U.B.	Avrg.± S.D.
4-layers 23% porous	25	14	96.26	84.55	108.69	3.91	2.63	5.54	86.69±27.26
	800	15	112.30	107.35	117.22	10.67	7.41	14.54	107.08±12.97
6-layers 23% porous	25	8	97.24	77.92	119.80	3.18	1.81	5.04	86.89±34.22
2-layers 23% porous	25	11	106.73	96.13	117.64	5.58	3.56	8.23	98.18±22.10
4-layers 20% porous	25	15	92.13	85.85	98.58	6.77	4.65	9.31	85.95±16.95
	800	15	108.57	97.76	119.86	4.61	3.27	6.19	99.42±23.25
4-layers 17% porous	25	15	99.62	90.30	109.91	4.73	3.38	6.61	91.25±21.89
	800	15	146.94	138.08	155.83	7.77	5.42	10.56	135.67±19.44
4-layers 7% porous	25	15	134.61	127.207	142.03	8.55	6.00	11.52	125.09±15.18
	800	15	145.45	132.65	158.67	5.25	3.68	7.11	130.40±26.60

T—Temperature
Avrg.—Average value
L.B.—lower 95% Confidence bound
U.B.—Upper 95% Confidence bound
S.D.—Standard Deviation
#—number of tested samples

The biaxial strength of reduced NiO/YSZ was determined at room temperature using samples with initial porosity of 23% that were subsequently reduced in a gas mixture of 4%H_2+96%Ar. Two groups of samples were tested: partially reduced with the fraction of reduced NiO of 55% and fully reduced with a fraction of reduced NiO of almost 100%. Also, the effect of the sample thickness and the number of layers on the mechanical properties were studied by evaluating samples with 2, 4 and 6 layers (Tables 3.5. and 3.6.) Altogether, 56 samples were tested. The biaxial strengths were analyzed using Weibull statistics and values of the characteristic strength and Weibull modulus are listed in Table 3.5 and 3.6 along with average strength values. Weibull plots for biaxial strengths are presented in Figs. 3.11–3.12.

3.4. WEIBULL ANALYSIS OF BIAXIAL STRENGTH OF REDUCED NIO/YSZ ANODE

As in the case of unreduced NiO/YSZ, the magnitude of the biaxial strength of fully and partially reduced NiO/YSZ does not depend significantly on the thickness of, or on number of layers in the samples. Comparing the results in Tables 3.4–3.6 and Figs. 3.11–3.12 for unreduced, partially reduced and fully reduced NiO/YSZ, it can be concluded that the magnitude of the biaxial strength of partially reduced samples with fraction of reduced NiO of 55 % is not significantly different from that of the unreduced samples. However, complete reduction of the NiO/YSZ samples leads to a decrease in the magnitude of the biaxial strength by almost 50 %.

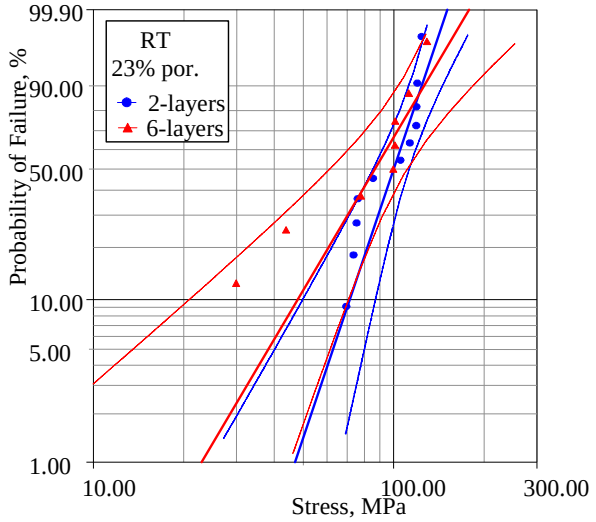

Fig. 3.6-3.10. Weibull plots for biaxial strength of NiO/YSZ samples as a function of testing temperature, porosity and number of layers. Dashed lines represent 95% confidence bounds.

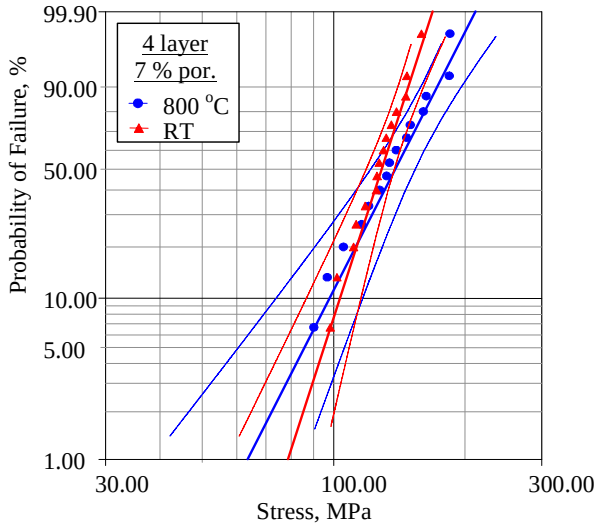

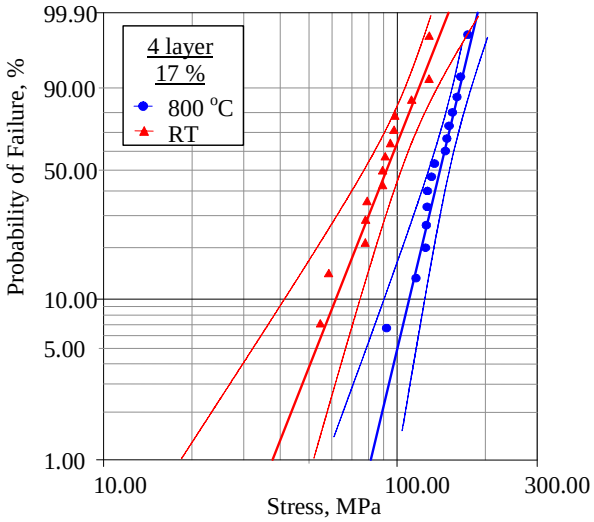

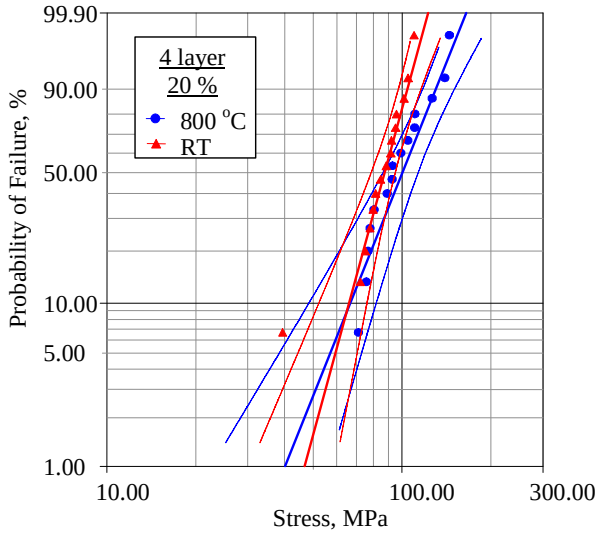

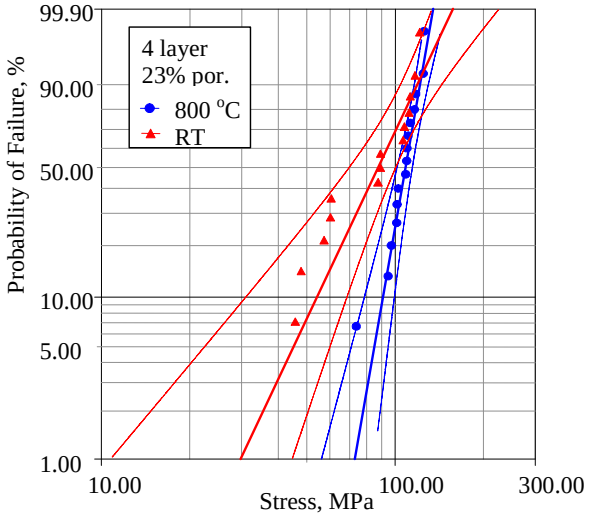

Table 3.5. Results of biaxial tests for fully reduced NiO/YSZ. Initial porosity of the samples was 23%, and porosity after reduction was measured to be 40%

	T, °C	#	Characterist. Strength, MPa			Weibull modulus			Strength, MPa
			Avrg.	L.B.	U.B.	Avrg.	L.B.	U.B.	Avrg.±S.D.
4-layers	25	14	55.32	49.68	61.62	4.33	3.14	5.98	50.52±12.42
6-layers	25	9	50.16	45.42	55.38	5.82	3.71	9.13	46.29±10.08
2-layers	25	9	76.40	69.09	83.88	6.52	3.98	9.88	71.00±13.65

T—Temperature
Avrg.—Average value
L.B.—lower 95% Confidence bound
U.B.—Upper 95% Confidence bound
S.D.—Standard Deviation
#—number of tested samples

Table 3.6. Results of biaxial tests for partial reduced NiO/YSZ. Initial porosity of the samples was 23%. Fraction of the reduced NiO was 55%

	T, °C	#	Characterist. Strength, MPa			Weibull modulus			Strength, MPa
			Avrg.	L.B.	U.B.	Avrg.	L.B.	U.B.	Avrg.±S.D.
4-layers	25	5	105.26	98.24	112.78	11.29	11.29	20.28	
6-layers	25	8	108.84	110.82	116.32	6.28	9.26	14.55	
2-layers	25	11	115.58	106.87	124.48	4.59	7.41	11.15	

T—Temperature
Avrg.—Average value
L.B.—lower 95% Confidence bound
U.B.—Upper 95% Confidence bound
S.D.—Standard Deviation
#—number of tested samples

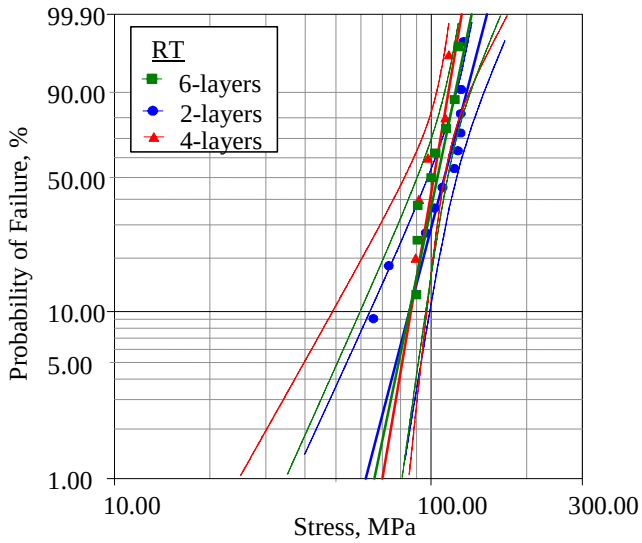

Fig. 3.11. Weibull plot for biaxial strength of 2, 4 and 4-layered partially reduced NiO/YSZ samples at room temperature. Dashed lines represent 95% confidence bounds.

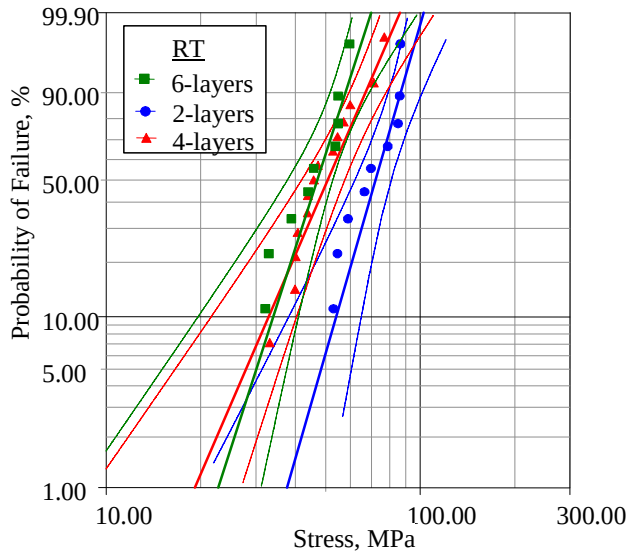

Fig. 3.12. Weibull plot for biaxial strength of 2, 4 and 4-layered completely reduced NiO/YSZ samples at room temperature. Dashed lines represent 95% confidence bounds.

3.5 FRACTURE TOUGHNESS OF ANODE AND ELECTROLYTE MATERIALS

The fracture toughness values of 4-layer 8YSZ and NiO/YSZ samples, which were determined at room temperature using Double-Torsion testing, are listed in Table 3.7. Samples were pre-cracked at a displacement rate of 0.01 mm/min and the formation of a sharp precrack was confirmed by Optical Microscopy. After precracking, all samples were tested at a constant displacement rate of 1 mm/min until failure. Results obtained for YSZ are in excellent agreement with those reported by others (1.61 MPa $m^{1/2}$) [5].

Table 3.7. K_{IC} of YSZ and NiO/YSZ at room temperature measured by Double-Torsion

	8YSZ	NiO/YSZ
K_{IC}, MPa $m^{1/2}$	1.65 ± 0.02	1.04 ± 0.13

4. SUMMARY

The kinetics of NiO reduction in a gas mixture of 4%H_2-96%Ar was investigated at temperatures between 600°C and 800°C. It was found that the initial reduction reaction followed linear kinetics at temperatures higher than 600°C until the reduction fronts reached the middle of the sample. After this point, the reaction rate decreased significantly and followed semi-parabolic kinetics. By performing interrupted reduction tests, it was possible to determine the dependence of the elastic properties and biaxial strength of NiO-YSZ anodes as a function of fraction of NiO reduction. In general, it was found that while the porosity of NiO-YSZ anodes increased with increasing fraction of NiO reduction, both the elastic modulus and biaxial strength decreased with increasing fraction of NiO reduction.

The effect of porosity and number of layers (thickness) on the biaxial strength of NiO-YSZ anodes was investigated at 20°C and 800°C and the results were analyzed using Weibull statistics. It was found that the strength of NiO-YSZ anodes decreased significantly when the porosity of the samples increased from 7% to 17%, but the strength appears to be insensitive to higher values of porosity up to 23%. It was also found that the strength of NiO-YSZ anodes is insensitive to the number of layers (2, 4 or 6) and that it has a mild temperature dependence.

The effect of number of layers was on the biaxial strength of YSZ electrolytes was investigated at temperatures between 20°C and 800°C. It was found that the strength of YSZ samples decreased significantly with increasing number of layers. Although the fractographic analysis of these test specimens has not been completed, preliminary observations indicate that delaminations might be responsible for the observed decrease in strength. It was also found that while the strength decreased from

20°C to 600°C, the strength increased at 800°C. Work is in progress to determine the mechanism(s) responsible for this behavior.

Raman spectroscopy and WDS have been used for chemical phase identification, and on-going work has been focused on using the former to determine stresses in SOFC materials.

5. REFERENCES

1. Sridhar S., Sichen D., and Seetharman S., "Investigation of the Kinetics of Reduction of Nickel Oxide and Nickel Aluminate by Hydrogen," *Z METALLKD* **85,** (1994) 616–620.
2. ASTM standard C1259-98.
3. A. C. Muller, B. Pei, A. Weber, and E. Ivers-Tiffee, HTMC IUPAC Jülich 2000, pp.1–4.
4. ASTM standard E 1461-01.
5. A. Atkinson and A. Selcuk, "Strength and Toughness of Tape-Cast Yttria-Stabilized Zirconia," *J. Am. Ceram. Soc.*, **83** (2000) p. 2029.